Nanoscale

Accepted Manuscript

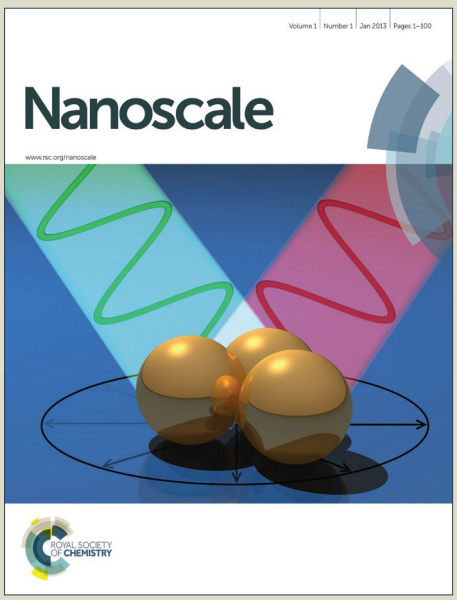

ROYAL SOCIETY OF CHEMISTRY

www.rsc.org/nanoscale

Cite this: DOI: 10.1039/c0xx00000x

www.rsc.org/xxxxxx

ARTICLE TYPE

Controlled thickness and morphology for highly efficient inverted planar heterojunction perovskite solar cells

Jun Xi,[#a] Zhaoxin Wu,[#*a] Hua Dong,[a] Bin Xia,[a] Fang Yuan,[a] Bo Jiao,[a] Lixin Xiao,[*b] , Qihang Gong[b] and Xun Hou[a]

Received (in XXX, XXX) Xth XXXXXXXXX 20XX, Accepted Xth XXXXXXXXX 20XX
DOI:

Recently, inverted planar heterojunction (PHJ) perovskite solar cells have been developed rapidly by numerous preparations and relative optimizations. Sequential solution deposition is easy to manipulate but difficult to control the thickness and morphology of perovskite films. In this article, we report an improved sequential deposition, named twice dipping-vapor solution deposition (TD-VSD) technology, to accurately achieve superior perovskite films. It is demonstrated that the morphology of peovskite films depended on the substrate temperatures as well as the dipping times. The resulting solar cells showed the power conversion efficiency as high as 11.77% based on the ideal thickness and morphology. This work provides a simple but effective fabrication to well control the perovskite films and enhance the power conversion efficiency for inverted PHJ solar cells.

Introduction

Since Miyasaka et al. first achieved a promising power conversion efficiency (PCE) by the materials of organolead trihalide perovskite,[1] hybrid organic/inorganic $MAPbX_3$ ($MA=CH_3NH_3$, X=I, Br or Cl) have drawn tremendous attention to all over the photovoltaic field in the recent years. Numerous superior properties of perovskite as the absorbers, including proper band gap (about 1.5 eV), exceptional absorption of visible light, long rang carrier transport lengths and high carrier mobilities, have been demonstrated by a series of referred mechanism research.[2-5] Moreover, the state of the art perovskite solar cells with a PCE of 19.3%, greatly overwhelmed other solar cells (such as organic photovoltaic (OPV), dye-sensitized solar cell (DSSC)).[6]

Meso-superstructured perovskite sensitized solar cells, evolved from DSSCs, have come up to relatively high PCEs before several years,[7-8] and have been rapidly accelerated by solution process.[9-12] Despite the advantages of easy-manipulating, some drawbacks and limitations of this structure are disappointing: the high treatment temperature of mesoporous scaffold, costly hole transportation materials 2,2',7,7'-tetrakis-(N,N-di-p-methoxyphenylamine)9,9'-spirobifluorene (spiro-OMeTAD) and poor reproducibility.[12-13] Surprisingly, low temperature planar heterojunction (PHJ) structures sandwiched by p-type and n-type layers, arising from organic film devices, have exhibited better device performances, avoided these shortages and could be utilized for commercialization even for flexible device.[14-17] However, the efficiency losses, structure defects and carrier recombination at the interfaces lead to worse performances.[15] Thus, a lot of optimizations have been reported as for following aspects: substitution of p-type layer (such as NiO, graphene oxide, CuSCN and so on),[18-23] interface modification,[24-25] tunning of perovskite procedure solution,[26-27] and vacuum deposition.[28-31] There is no doubt that the aim of above optimization is to support continuous and smooth perovskite films.

In previous reports, three fabrications of perovskite films were employed.[7,32-33] 1) Dual-source vacuum deposition contributes to a compact and flat film, but needs advanced apparatus and is difficult to detect the deposition rates of CH_3NH_3I.[28] 2) One-step spin-coating easily forms incomplete and non-uniform perovskite films.[10,34-35] What's more, a critical environment is inevitable for this process. 3) Sequential solution deposition leads to large crystalline grain, hard controls the crystal sizes and results to a inferior device performance.[36] Especially for fabricating inverted PHJ structures, thicker n-type layers (such as C60, PCBM and other fullerene derivatives) are hardly realized compared to spiro-OMeTAD (in TiO_2 mesoporous structure), whereas are indispensible for the rough perovskite films by sequential solution.[8,24] Recently, Tang et al. have realized a PCE of 7.6% by sequential deposition.[22] Furthermore, a higher PCE of 9.11% was reported with NiO nanocrystal by the group of Yang.[23] But thinner n-type layers would improve the conductivity and accordingly lead to a better device performance.[37-39] Consequently, an appropriate thickness of n-type layers is also paramount to achieve preferable device performance. It is not easy, however, to obtain excellent device parameters for PHJ structure by sequential deposition due to the demerits mentioned above.

In this work, we establish an improved sequential deposition for inverted PHJ perovskite solar cells by vapor solution deposition (VSD) approach, which is dipping vapor deposition (VD) PbI_2 films into CH_3NH_3I solution for deposition. We find that twice dipping VSD (TD-VSD) is more sufficient and effective than once dipping VSD (OD-VSD), but third dipping VSD (T'D-VSD) is detrimental for perovskite film. Consequently, TD-VSD is favorable for PHJ devices. It is notable that DMF will dissolve

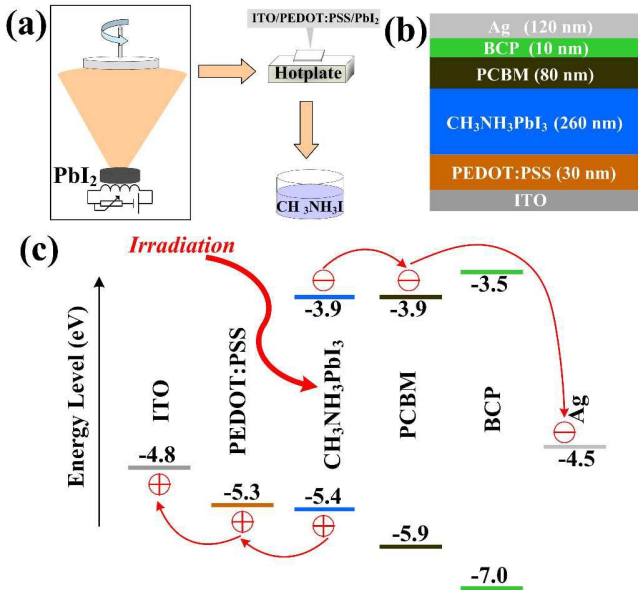

Fig. 1 (a) Schematic procedure of OD-VSD technology. (b) Device structure of prepared PHJ solar cells. (c) Corresponding energy levels diagram as well as carrier transportation under solar illumination.

part of PEDOT:PSS films by traditional sequential solution deposition.[23] The VD PbI_2 could guard the PEDOT:PSS films. And fortunately, resulting $CH_3NH_3PbI_3$ thickness can be precisely controlled by vacuum deposition. In addition, the substrate temperatures could impact the perovskite morphology. The champion solar cells show power conversion efficiencies as high as 11.77% by further optimizing other conditions of the technology, which are superior to the similar sequential deposition with the same architectures (about 5% to 9%).[22-23] We also reveal the importance of the absorption and morphology for the inverted PHJ perovskite solar cells.

Results and discussion

1. OD-VSD for perovskite solar cells

The schematic procedure of OD-VSD technology (**Fig. 1**a) is similar to that of the traditional sequential solution deposition, and detailed process can be found in the experimental section. The device structure and the energy levels diagram of PHJ solar cells developed in our work are shown in **Fig. 1**b and **1**c. PbI_2 powders were heated to its sublimation temperature to form transport yellow films. The PbI_2 film was further characterized by X-ray diffraction (XRD) in **Fig. 2**a. The predominant peak at 12.6 ° of the XRD pattern is ascribed to the (001) lattice plane of crystallized PbI_2. And the inset scanning electron microscopy (SEM) image of **Fig. 2**a shows continuous and smooth PbI_2 film consist of a multitude of homogeneous crystals. The substrates were heated with different temperatures (including RT, 40 ℃, 50 ℃, 60 ℃, 70 ℃ and 80 ℃) for 2 min, and then immersed into CH_3NH_3I solution to form dark brown perovskite ($CH_3NH_3PbI_3$). On account of volatility of DCM (dichloromethane) and the poor solubility of perovskite in DCM,[40] the samples ITO/PEDOT:PSS/$CH_3NH_3PbI_3$ were cleaned with IPA (2-propanol) and DCM sequentially to eliminate the MAI trace.

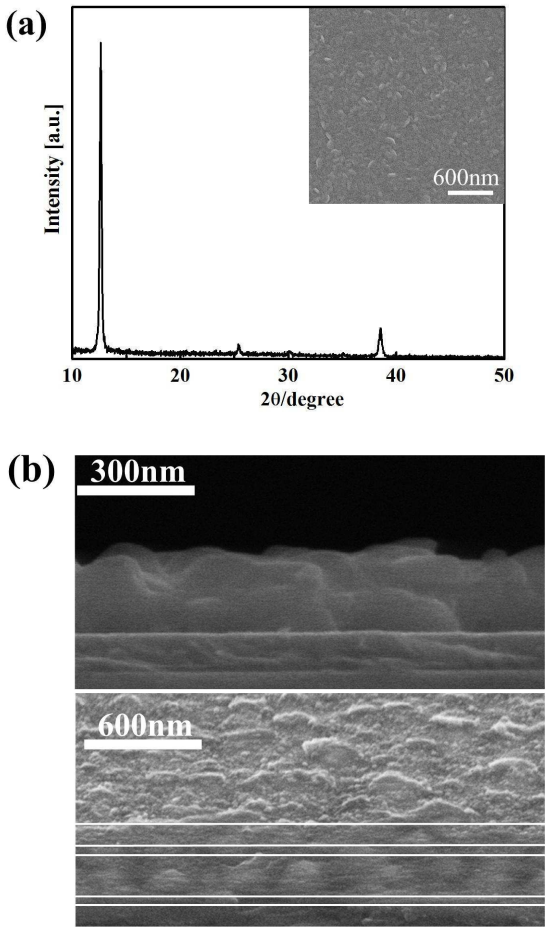

Fig. 2 (a) XRD pattern of the VD PbI_2 film. (inset: SEM images) (b) The cross sectional SEM images of $CH_3NH_3PbI_3$ film and the device structure.

Compared with traditional sequential solution deposition, this process can be operated easily and time-saving due to avoiding annealing. The above image of **Fig. 2**b exhibits an approximate 260nm thickness of a continuous $CH_3NH_3PbI_3$ film. The prepared perovskite were next protected with 80 nm PCBM by spin-coating. Eventually, the devices were deposited with 10 nm BCP and 120 nm Ag cathode sequentially to complete. The BCP layer acts as the role of hole blocking on account of its deeper HOMO. The subjacent image of **Fig. 2**b also shows the final structure of prepared PHJ solar cell device by OD-VSD technology.

The OD-VSD procedure leads to multifarious films composed of different $CH_3NH_3PbI_3$ crystal sizes upon the PEDOT:PSS layer. That is, interestingly, the temperature of substrates plays an important role for the $CH_3NH_3PbI_3$ morphology. As demonstrated in the SEM images (**Fig. 3**a), the mean crystal size of $CH_3NH_3PbI_3$ is ~146 nm at RT (room temperature), ~173 nm at 40 ℃, ~185 nm at 50 ℃, ~198 nm at 60 ℃, ~293 nm at 70 ℃ and ~ 344 nm at 80 ℃, respectively. The plot of the crystal mean size as a function of substrate temperatures, depicted in **Fig. 3**b, suggests no linear rule. It can be recognized that much greater crystal size, rougher surface and lower coverage of $CH_3NH_3PbI_3$ layer are determined above 60 ℃. We can conclude that the variation of $CH_3NH_3PbI_3$ crystal size is almost consistent with

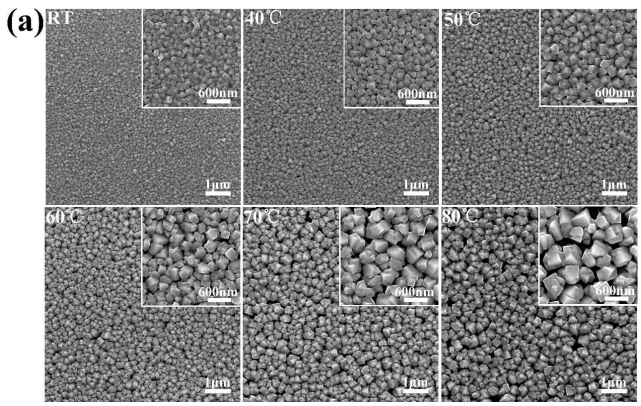

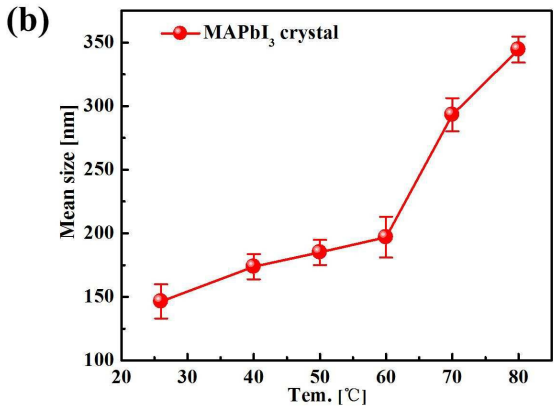

Fig. 3 (a) Top-view SEM images of the OD-VSD $CH_3NH_3PbI_3$ films upon the PEDOT:PSS layer at different substrate temperatures. (b) Plot of mean size (nm) of $CH_3NH_3PbI_3$ crystal as a function of substrate temperatures.

.

the temperature increase. Regardless of temperature, a resulting $CH_3NH_3PbI_3$ (260nm) film is approximately 2.6 times as thick as the pristine PbI_2 film (120nm). Park et al. considered that the growth rate along the c-axis is slower than the a-b plane, and scaffolds are essential to limit the $CH_3NH_3PbI_3$ size in traditional TiO_2 structure.[41] Nevertheless, we achieved well controlled crystal size and morphology upon planar PEDOT:PSS film.

In order to estimate the properties of perovskite, a group of PHJ solar cells, with the structure: ITO (100 nm)/PEDOT:PSS (30 nm)/$CH_3NH_3PbI_3$ (260 nm)/PCBM (80 nm)/BCP (10 nm)/Ag (120 nm), had been fabricated. **Fig. 4**a shows the average performance of the devices prepared at various substrate temperatures. The corresponding photovoltaic parameters are summarized in **Table 1**. For the RT case, all the values are inferior to other cases. When the temperature reached 50 to 70 ℃, all the devices exhibited distinguished performances, in which the triumph PCE of 6.76% was achieved. Unfortunately, deteriorated cells at 80 ℃ with a PCE of 3.29% are delivered due to particularly poor coverage of perovskite films. For investigating the dependence of device performances on temperature, the variation of each parameter as a function of substrate temperatures is plotted in **Fig. 4**b.

There is a positive correlation between the photovoltaic parameters and the temperature. 1) The value of FF is improved

Table 1 The average photovoltaic parameters of the ITO/PEDOT:PSS/ $CH_3NH_3PbI_3$/PCBM/BCP/Ag devices by OD-VSD technology.

Tem.[℃]	J_{sc} [mA/cm^2]	V_{oc} [V]	FF [%]	PCE [%]
RT	4.92	0.65	37.5	1.20
40	10.20	0.79	50.5	4.07
50	12.20	0.87	56.6	6.01
60	12.96	0.87	57.5	6.49
70	13.44	0.89	56.5	6.76
80	8.52	0.82	47.1	3.29

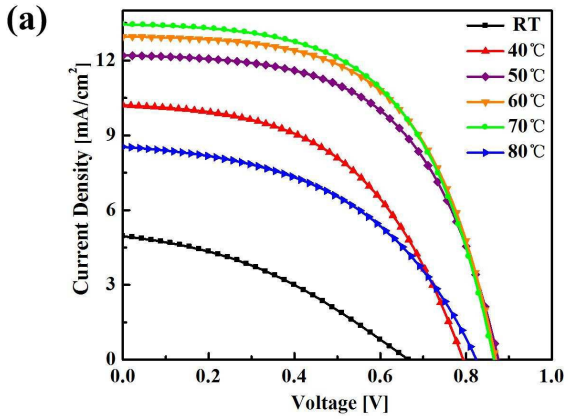

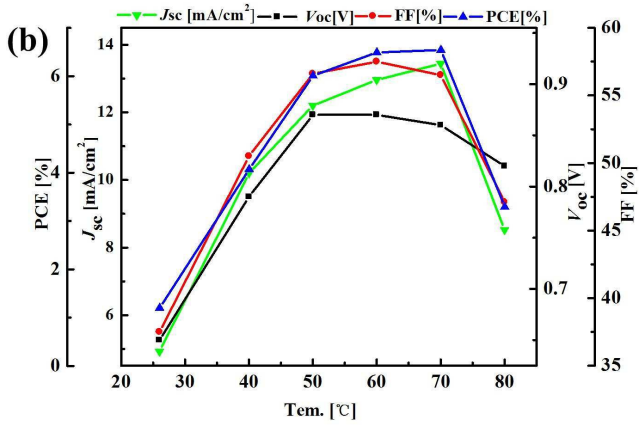

Fig. 4 (a) Current density-Voltage (J-V) curves for devices fabricated at various substrate temperatures by OD-VSD technology measured under 1 sun AM 1.5G illumination. (b) the variation of J_{sc}, V_{oc}, FF and PCE as a function of the substrate temperatures.

with the temperatures increase, and is obviously reduced until 80 ℃. This can be explained for the reason: more grain boundaries at lower temperatures contribute to increasing series resistance and hence terrible FF, despite better coverage.[42] As for 80 ℃, coarse and imperfect perovskite film will lead to poor FF. 2) The variation of V_{oc} is similar to that of FF. Although the V_{oc} is determined by the difference between the LUMO of PCBM layer and HOMO of PEDOT:PSS layer, there still remains some factors affecting the V_{oc}. At higher temperatures, internal

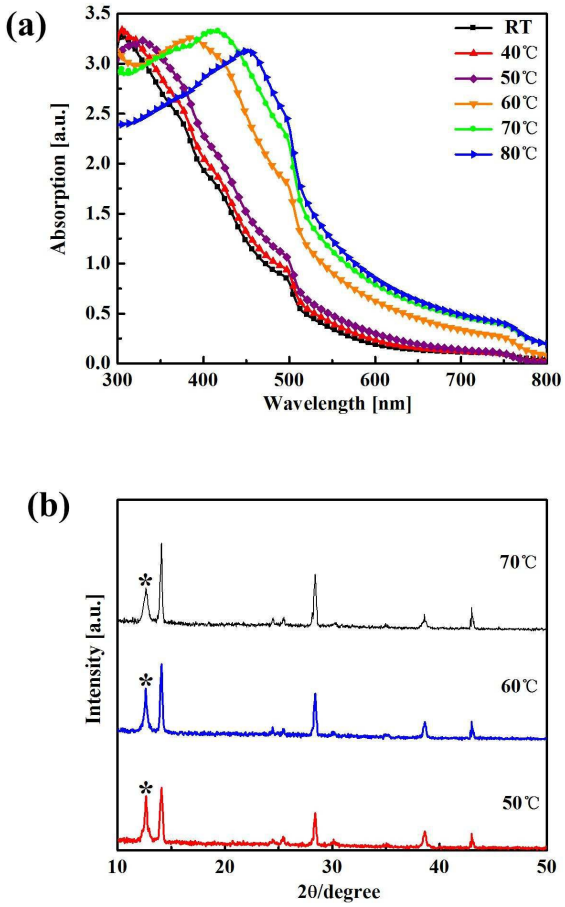

Fig. 5 (a) Absorption spectra and (b) XRD patterns (* represents the (001) plane of PbI_2) of ITO/PEDOT:PSS/$CH_3NH_3PbI_3$ films prepared by OD-VSD technology at various substrate temperatures.

shunting at uncovered areas is likely caused by poorer coverage and hence results in inferior V_{oc}. At lower temperatures, what's more, the more residual PbI_2 (will be discussed later) contribute to lower V_{oc}. 3) The improvement of J_{sc} is predominant among the overall performances enhancement along the temperature increase (except for 80 ℃). The reasons for the higher temperature leading to the greater J_{sc} are confirmed for the following aspects: First and foremost, it is determined that the absorption spectra gradually enhanced in mid-long wavelenghth as the substrate temperatures increase in **Fig 5**a. On one hand, the utilizations of visible light can be improved when the substrate temperature climbs up. Considering the similar film thickness, the increased absorption presumably results from light scattering of the larger-sized $CH_3NH_3PbI_3$ crystals of rough surface.[41,43] What's more, the increased absorption will contribute to more free carriers, which results in corresponding J_{sc} increase.[29] On the other hand, continuous and homogenous perovskite film composed of larger-sized crystals will boost carrier transport and improve carrier-diffusion properties.[44-45]

Focused on the outstanding devices prepared at 50-70 ℃, the ITO/PEDOT:PSS/$CH_3NH_3PbI_3$ films are further determined by XRD (**Fig. 5**b). All of the XRD patterns of 50-70 ℃ show a set of diffraction peaks of tetragonal $CH_3NH_3PbI_3$ structure at 14.08°, 28.4° and 43.01°, assigned to (110), (220) and (330) planes, respectively. For 50 ℃, the signal intensity at 12.6° is still evident, indicating risidual PbI_2. When the temperatures of samples are elevated to 60 ℃ and 70 ℃, the XRD pattern of $CH_3NH_3PbI_3$ manifests that the production of perovskite is improved along with temperatures increase. In the meanwhile, prestine PbI_2 declines apperently. Hence, the crystal properties presented by XRD also account for the improvements of PCE. However, we realize that a proption of PbI_2 still remain, which is detrimental for the device performance. In order to completely transfrom the PbI_2 to $CH_3NH_3PbI_3$, we further attempted to develop the TD-VSD technology for improving the OD-VSD technology.

2. TD-VSD for perovskite solar cells

To simplify the name, OD is named for OD-VSD, while TD is named for TD-VSD. The proceudre of TD is similar to that of OD. In short, after dipping into CH_3NH_3I solution and washing, the substrates with perovskite were heating at the same temperature for 3min, and were conducted as the former perovskite preparation again.

For comparison, the morphology of perovskite films were first determined by the SEM. **Fig. 6**a shows denser crystals and fewer holes of $CH_3NH_3PbI_3$ films by TD than OD at the same temperature. Actually, we can find that lots of tiny crystals fill

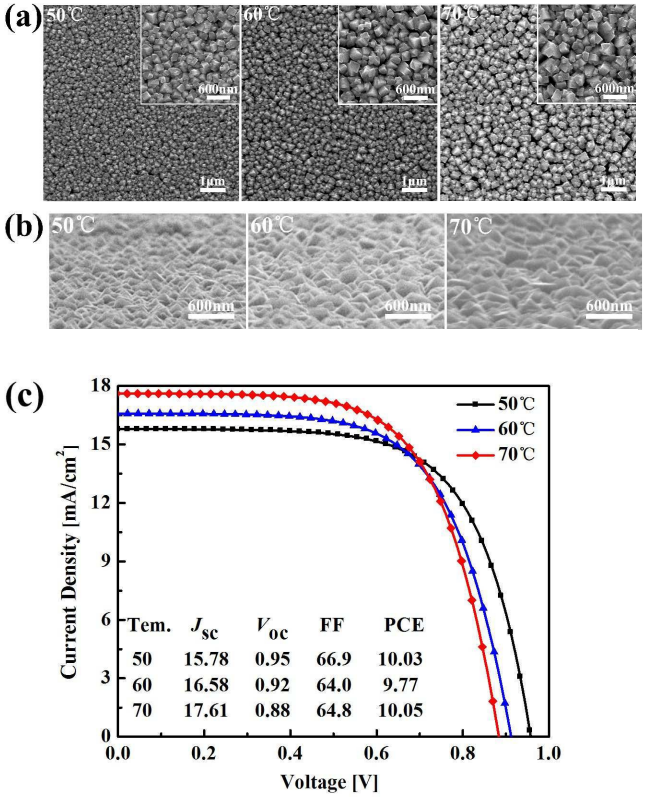

Fig. 6 (a) Top-view and (b) cross sectional SEM images of the TD-VSD $CH_3NH_3PbI_3$ films upon the PEDOT:PSS layer at different substrate temperatures. (c) Current density-Voltage (J-V) curves for devices fabricated at various substrates temperatures by TD-VSD technology measured under 1 sun AM 1.5G illumination. The inset summarizes the average parameters.

the intervals of original larger crystals to diminish the perovskite holes in OD. The cross sectional images (**Fig. 6**b) further show the prepared continuous and quasi-smooth $CH_3NH_3PbI_3$ films, and also the gradual enlarged crystal size as temperature increase. Accordingly, the p-type layer (PEDOT:PSS) and the n-type layer (PCBM) will be in well contact with perovskite films, which will reduce internal shunting as well as leakage current for the prepared device. But film thickness still keeps same (**Fig. S1**†).

A group of devices of the same architecture by TD, in a similar manner of OD procedure as described previously, were prepared to investigate the benefits of TD procedure for the substrates with 50 ℃, 60 ℃ and 70 ℃. **Fig. 6**c shows the current density-voltage curves and the average photovoltaic parameters. Apparently, such solar cells exhibit amazing performances surpassing the former results by OD. At higher temperatures, a little decrease of V_{oc} would be ascribed to the tiny holes of perovskite films. Most importantly, the J_{sc} varies from 12.20 mA/cm^2 to 15.78 mA/cm^2 at 50 ℃, from 12.96 mA/cm^2 to 16.58 mA/cm^2 at 60 ℃, and from 13.89 mA/cm^2 to 17.61 mA/cm^2 at 70 ℃. We then define that the ΔJ_{sc} equals to [J_{sc} (TD)—J_{sc} (OD)]/J_{sc} (OD). The value of ΔJ_{sc} is 29.3% at 50 ℃, 27.9% at 60 ℃, and 26.8% at 70 ℃, respectively, which suggests that TD procedure could lead to a much higher short-circuit current density.

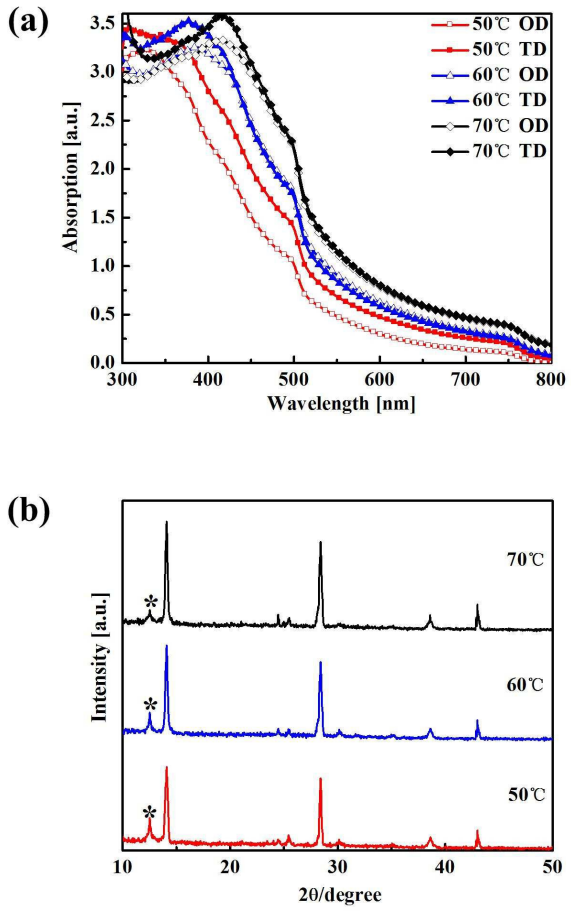

Fig. 7 (a) Absorption spectra and (b) XRD patterns (* represents the (001) plane of PbI_2) of ITO/PEDOT:PSS/$CH_3NH_3PbI_3$ films prepared by TD-VSD technology at various substrate temperatures.

The resulting higher ΔJ_{sc} at 50 ℃ can be also interpreted by the absorption of perovskite films. **Fig. 7**a presents the absorption spectra comparison for OD and TD of the ITO/PEDOT:PSS/$CH_3NH_3PbI_3$ films. Greater enhancement of absorption covers almost all over the visible light at 50 ℃. However, slighter enhancements appear only from 300nm to 425nm at 60 ℃, and from 300nm to 450nm at 70 ℃.

In order to further determine the benefits of TD, XRD patterns of ITO/PEDOT:PSS/$CH_3NH_3PbI_3$ films fabricated by TD are shown in **Fig. 7**b. Compared with the XRD patterns of OD, enhancement of the intensity of $CH_3NH_3PbI_3$ is much strong, which indicates almost adequate conversion of PbI_2. The improvement of J_{sc} is also deserved. And the favorable crystals of perovskite prepared at higher temperatures are also in consistent with the SEM images.

3. Mechanism

To further demonstrate the nature of perovskite formation, another group of perovskite by dipping the substrates covered with PbI_2 at 50 ℃, 60 ℃, 70 ℃, and even 80 ℃ for three times were prepared. T'D is named for the third dipping.

Distinct variation of absorption spectra can be found between OD and T'D in **Fig. 7**a. But almost no obvious variation apprears between TD and T'D in **Fig 8**a. This odd result reminds us that

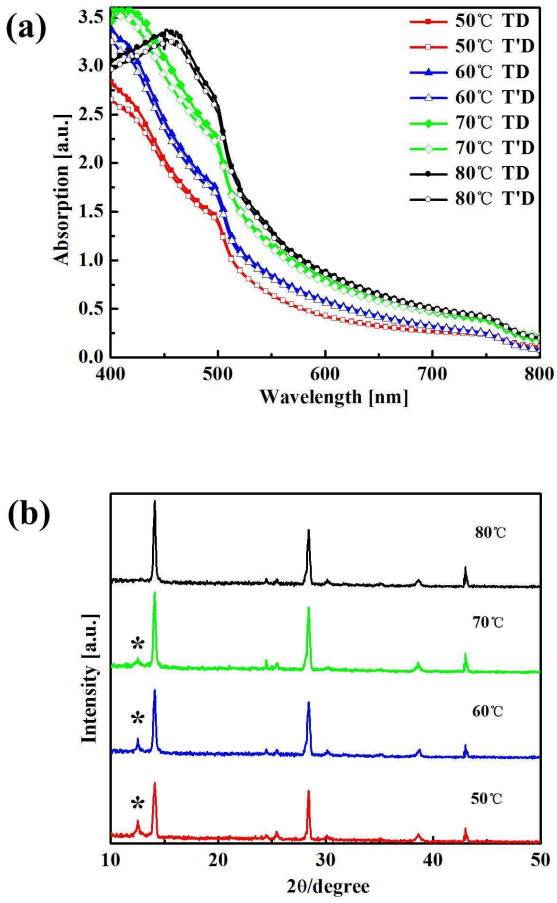

Fig. 8 (a) Absorption spectra and (b) XRD patterns (* represents the (001) plane of PbI_2) of ITO/PEDOT:PSS/$CH_3NH_3PbI_3$ films prepared by T'D procedure at various substrate temperatures.

the perovskite formation may be limited by some factors.

Fig. 8b exhibits XRD patterns of T'D at various substrate temperatures. The corresponding intensities of diffraction peaks can be found in **Table S1**†. From OD to TD, all the intensities of 12.6° decline apparently, meanwhile the intensities of 14.08° increase strongly. This indicates the residual PbI_2 was diminished to some extent. From TD to T'D, the intensities at 12.6° nearly remain but the diffraction peaks of perovskite all decrease slightly. Speculated from the XRD patterns, the conversion into perovskite degree has been aggravated by TD, but ceased even reduced by T'D. And the PbI_2 will be completely transformed into perovskite at 80 ℃. Similarly, coverage rates are improved from OD to TD, but almost remain from TD to T'D from the top-view SEM images (**Fig. S2**†).

The devices with the same layout were prepared to determine the effect of T'D. **Fig. 9**a presents the current density-voltage curves and the average photovoltaic parameters. However, frustrating peformances were obtained in comparison to TD. This unfavorable results indicates that the perovskite film made by T'D is really deteriorated, which is in accordance with film characterization. Though 80 ℃ will lead to complete conversion,

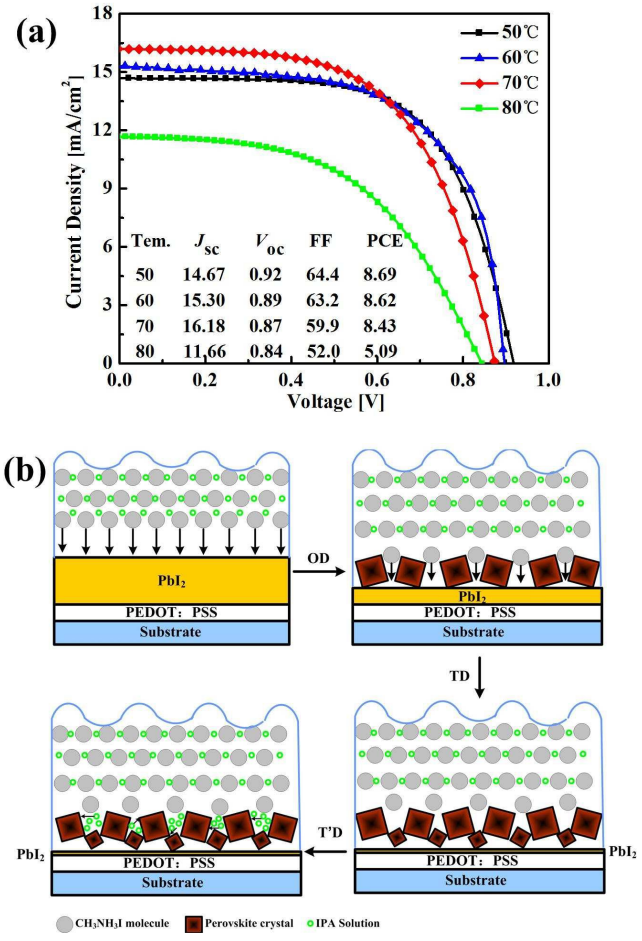

Fig. 9 (a) Current density-Voltage (J-V) curves for devices fabricated at various substrates temperatures by T'D procedure measured under 1 sun AM 1.5G illumination. The inset summarizes the average parameters. (b) Illustration of the mechanism stages for perovskite formation.

the terrible film surface destroys the device work. We can infer that better interface is more beneficial for device performance than little PbI_2.

From all the former results, the perovskite mechanism can be speculated in following aspects:

1) For OD procedure, when the substrates with different temperatures were immersed into CH_3NH_3I solution, the CH_3NH_3I molecules immediately react with PbI_2 film. Due to the more condense density of vapor PbI_2 film, the reaction degree and rate will be limited but improved by temperatures. However all the PbI_2 still cannot be completely transformed into perovskite.

2) For TD procedure, the upper layers of substrate are composed of perovskite-PbI_2 films. There are lots of major holes as well as intervals existed between the large-sized crystal of perovskite. The CH_3NH_3I molecules will filter into these defects and continue to react with residual PbI_2 films. Consequently, lots of tiny crystals appears between the bigger crystals regardless of IPA little corrosion,

3) For T'D procedure, the perovskite crystals are denser and show almost no defects. The CH_3NH_3I molecules hardly meet with the little residual PbI_2 (except for 80 ℃). What's more, excess IPA solution may partially corrode the perovskite by TD due to the substrate's third immersion. The eventual results also support the possible reason.

Regardless of complicated factors by now, this primary mechanism is established. As an example, **Fig. 9**b shows the illustration of the mechanism stages for PbI_2 conversion into perovskite.

4. Device optimization

Finally, we maintained the architecture to optimize the solar cells by adjusting the PbI_2 thickness (120nm) with the TD procedure. The average devices performances are shown in **Table 2**. All the devices prepared with 150nm PbI_2 exhibit better performances, especially higher J_{sc}. The maximum J_{sc} of 18.58 mA/cm^2 has almost been comparable to the J_{sc} of the excellent p-i-n PHJ devices reported (from 16.12 to 19.2 mA/cm^2).[24,29,30] What's more, the devices fabricated with 150nm PbI_2 by TD manifested well FF (above 60%) as well as high V_{oc} (about 1.0 V), which can be attributed for the robust interfaces between the perovskite films and the PCBM layers.

Fig. 10a demonstrates the current density-voltage curves of the champion solar cells, achieving at 50 ℃, measured under 1 sun AM 1.5G illumination and in the dark. The optimizing highest PCE of 11.77% was realized, yielding a J_{sc} of 17.28 mA/cm^2, V_{oc}

Table 2 The average photovoltaic parameters of the ITO/PEDOT:PSS/ $CH_3NH_3PbI_3$/PCBM/BCP/Ag devices by OD-VSD technology.

Tem.[℃]	PbI_2 thickness [nm]	J_{sc} [mA/cm^2]	V_{oc}[V]	FF[%]	PCE[%]
50	90	15.14	0.91	63.8	8.79
	150	16.66	1.03	65.1	11.17
60	90	15.83	0.88	61.7	8.59
	150	17.12	1.00	62.1	10.63
70	90	16.95	0.84	59.6	8.48
	150	18.58	0.98	60.3	10.97

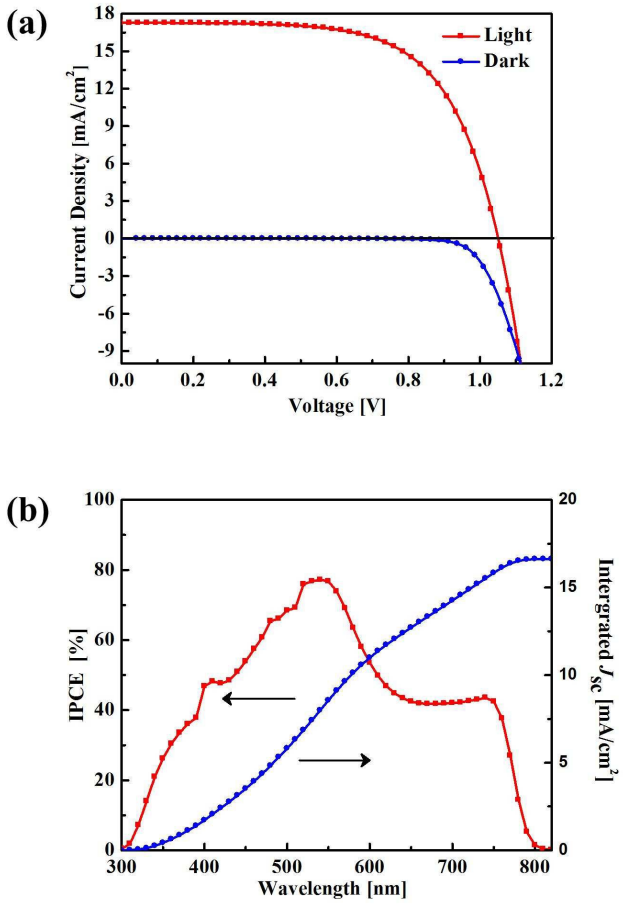

Fig. 10 (a) Current density-Voltage (J-V) curves and (b) IPCE spectrum for champion solar cells fabricated at 50 ℃ by TD-VSD technology measured under 1 sun AM 1.5G illumination and in the dark.

of 1.05 V and FF of 64.8%, respectively. Histograms of the cell performance characteristics are shown **Fig. S3**†. It is noted that the relative standard deviations of the PCE was only 0.27, which indicates excellent reproducibility of the devices by TD-VSD technology. The high open-circuit potential also implies negligible surface defects and sub-bandgap states in the perovskite film.[30] In the meanwhile, the hysteresis of scan process, existed in our devices (**Fig. S4**†), shows a 11% deviation of PCE from reverse to forward. The incident photon-to-current conversion efficiency (IPCE) spectrum (**Fig. 10**b) exhibits generation of photocurrent starts at 800 nm, in agreement with the bandgap of the $CH_3NH_3PbI_3$, and reaches peak values in the short-wavelength region of the visible spectrum. The integrated current density derived from the EQE spectra in **Fig. 10b** is in close to the J_{sc} measured under simulated sunlight**.**

Conclusion

Highly efficient inverted PHJ perovskite solar cells were achieved and optimized by a novel TD-VSD technology. We emphasized the importance of substrates (covered with PbI_2) temperatures on the resulting $CH_3NH_3PbI_3$ crystal sizes and uniformity, and find that large-sized crystals will result in stronger absorption in mid-long wavelength. Furthermore, the primary mechanism of perovskite formation is established by employing dipping substrates for different times. It is notable that optimizing procedure revealed more sufficient conversion of VD PbI_2 films. When an appropriate temperature is established, the favorable $CH_3NH_3PbI_3$ films with fewer defects would support better interfaces and improve carrier transport. For this controlled thickness and morphology of $CH_3NH_3PbI_3$ films, a champion solar cell prepared in this way performed the highest PCE of 11.77 %.

Experimental

Preparation of Materials

Methylammonium iodide (MAI) was synthesized by a previous literature.[8] In brief, 24 mL methylamine solution (33 wt% in ethanol, Sigma Aldrich) and 10 mL hydriodic acid (57 wt% in water, Sigma Aldrich) were diluted by 100mL ethanol in a 250 mL round bottom flask by constant stirring at 0 ℃ for 2 hours. The precipitate of CH_3NH_3I was gained by rotary evaporation at 40 ℃ and washed with dry diethyl ether until the solid became white. The final product was dried at 60 ℃ in a vacuum oven for 24h. PbI_2 (99.999 wt%) was purchased from Alfa. PEDOT:PSS (CLEVIOS PH 1000) solution and PCBM were acquired from Haraeus and Solenne, respectively.

Fabrication of solar cells

1) Pretreatment: ITO glass substrates were cleaned sequentially by detergent, pure water, acetone for 20 min. The dried substrates were treated with ultraviolet ozone plasma for 5 min for further clean. PEDOT:PSS solution (dissolved with deionized water in a mixture ration of 1:3) were spun at 1000 rpm for 30s and annealed at 120 ℃ for 20 min.

2) Perovskite fabrication: For OD-VSD, we transferred the substrates coated PEDOT:PSS to a vacuum chamber. The PbI_2 films of 90nm, 120nm or 150nm, were sublimated under a pressure of 10^{-5} mbar at a rate of 1.0 Å/s and resultant substrates were placed into the N_2-filled glovebox. Kept at room temperature, or heated for 2 min at 40, 50, 60, 70 and 80 ℃ respectively, the ITO/PEDOT:PSS/PbI_2 substrates were immersed into a CH_3NH_3I solution (10 mg/mL in 2-propanol) for 1 min, followed by washing with 2-propanol and dichloromethane. For TD-VSD, this group was implemented by the same process as OD-VSD. Moreover, the prepared perovskite films were repeated by heating, dipping and washing. For T'D-VSD, the same process was repeated for the third time.

3) Device achievements: Almost 80nm p-type films were deposited by spin-coating PCBM solution (30 mg/ml in chlorobenzene) at 2000 rpm for 30s. Eventually, the devices were completed by consecutively vacuum deposited BCP (10 nm) and Ag cathode (120 nm) under 10^{-5} mbar.

Characterization

Perovskite films for absorption measurements, SEM, AFM and XRD were prepared by the same fabrication conditions for the layer structures configured as: glass substrate/ITO/PEDOT:PSS/$CH_3NH_3PbI_3$. The absorption spectra were acquired on a UV-vis spectrophotometer (Fluoromax 4,

HORIBA Jobin Yvon, USA). The morphology were investigated by a scanning electron microscopy (SEM) (Quanta 250, FEI). The crystalline structures were performed by a X-ray diffraction (XRD) (D/MAX-2400, Rigaku, Japan) with Cu Kα radiation.

Device characteristics were evaluated in ambient under a AAA solar simulator (XES-301S, SAN-EI Electric. Co. Ltd.), AM 1.5G illumination with an intensity of 100 mW/cm^2 (1 sun, calibrated by a NREL-traceable KG5 filtered silicon reference cell). Meanwhile, the current density-voltage (J-V) curves were measured by a Keithley digital source meter (Model 2602). The scan rates of the planar heterojunction perovskite solar cell current-voltage curves was performed by 0.5 V/s starting from -0.1 V to 1.2 V. The Incident Photon-to-current Conversion Efficiency (IPCE) spectra were obtained by the solar cell quantum efficiency measurement system (SolarCellScan 100, Zolix instruments. Co. Ltd). The area of each device, calibrated by the shadow mask, was 9.00 mm^2.

Acknowledgements

This work was financially supported by Basic Research Program of China (2013CB328705), National Natural Science Foundation of China (Grant Nos. 61275034), Ph.D. Programs Foundation of Ministry of Education of China (Grant No. 20130201110065). The SEM work was done at International Center for Dielectric Research (ICDR), Xi'an Jiaotong University, Xi'an, China; The authors also thank Ms. Dai for her help in using SEM.

Notes and references

[#] *These authors contributed equally to this work.*

[a] *Key Laboratory of Photonics Technology for information, Key Laboratory for Physical Electronics and Devices of the Ministry of Education, School of Electronic and Information Engineering, Xi'an Jiaotong University, Xi'an 710049, P. R. China*
Tel: +86-29-82664867
E-mail: zhaoxinwu@mail.xjtu.edu.cn

[b] *State Key Laboratory for Mesoscopic Physics and Department of Physics, Peking University, Beijing 100871, P. R. China*
E-mail: xiao66@pku.edu.cn

1 A. Kojima, K. Teshima, Y. Shirai and T. Miyasaka, *J. Am. Chem. Soc.*, 2009, 131, 6050-6051.
2 S. D. Stranks, G. E. Eperon, G. Grancini, C. Menelaou, M. J. P. Alcocer, T. Leijtens, L. M. Herz, A. Petrozza and H. J. Snaith, *Science*, 2013, 342, 341-344.
3 G. Xing, N. Mathews, S. Sun, S. S. Lim, Y. M. Lam, M. Gräztel,S. Mhaisalkar and T. C. Sum, *Science*, 2013, 342, 344-347.
4 T. Leijtens, J. Lim, J. Teuscher, T. Park and H. J. Snaith, *Adv. Mater.*, 2013, 25, 3227-3233.
5 C. Wehrenfennig, G. E. Eperson, M. B. Johnston, H. J. Snaith and L. M. Herz, *Adv. Mater.*, 2014, 26, 1584-1589.
6 H. Zhou, Q. Chen, G. Li, S. Luo, T.-B. Song, H.-S. Duan, Z. Hong, J. You Y. Liu and Y. Yang, *Science*, 2014, 345, 542-546.
7 H. S. Kim, C. R. Lee, J. H. Im, K. B. Lee, T. Moehl, A. Marchioro, S. J. Moon, R. Humphry-Baker, J. H. Yum, J. E. Moser, M. Gräztel and N. G. Park, *Sci. Rep.*, 2012, 2, 591.
8 M. M. Lee, J. Teuscher, T. Miyasaka, T. N. Murakami and H. J. Snaith, *Science*, 2012, 338, 643–647.
9 J. T.-W. Wang, J. M. Ball, E. M. Barea, A. Abate, J. A. Webber, J. Huang, M. Saliba, I. Mora-Sero, J. Bisquert, H. J. Snaith and R. J. Nicholas, *Nano Lett.*, 2014, 14, 724-730.
10 G. E. Eperon, V. M. Burlakov, P. Docampo, A. Goriely and H. J. Snaith, *Adv. Funct. Mater.*, 2014, 24, 151–157.
11 A. Dualeh, N. Tetreault, T. Moehl, P. Gao, M. K. Nazeeruddin and M. Gräztel, *Adv. Funct. Mater.*, 2014, 24, 3250-3258
12 J. M. Ball, M. M. Lee, A. Hey and H. J. Snaith, *Energy Environ. Sci.*, 2013, 6, 1739.
13 N.-G. Park, *J. Phys. Chem. Lett.*, 2013, 4, 2423-2329.
14 J.-Y. Jeng, Y.-F. Chiang, M.-H. Lee, S.-R. Peng, T.-F. Guo, P. Chen and T.-C. Wen, *Adv. Mater.*, 2013, 25, 3727-3732.
15 J. You, Z. Hong, Y. Yang, Q. Chen, M. Cai, T.-B. Song, C.-C. Chen, S. Lu, Y. Liu, H. Zhou and Y. Yang, *ACS Nano*, 2014, 8, 1674-1680.
16 C. Roldan-Carmona, O. Malinkiewicz, A. Soriano, G. M. Espellargas, A. Garcia, P. Reinecke, T. Kroyer, M. L. Dar, M. K. Nazeeruddin and H. J. Bolink, *Energy Environ. Sci.*, 2014, 7, 994-997.
17 Y.-F. Chiang, J.-Y. Jeng, M.-H. Lee, S.-R. Peng, P. Chen, T.-F. Guo, T.-C. Wen, Y.-J. Hsu and C.-M. Hsu, *Phys. Chem. Chem. Phys.*,2014, 16, 6033-6040.
18 J.-Y. Jeng, K.-C. Chen, T.-Y. Chiang, P.-Y. Lin, T.-D. Tsai, Y.-C. Chang, T.-F. Guo, P. Chen, T.-C. Wen and Y.-J. Hsu, *Adv. Mater.*, 2014, 26, 4107-4133.
19 K.-C. Wang, P.-S. Shen, M.-H. Li, S. Chen, M.-W. Lin, P. Chen and T.-F. Guo, *ACS Appl. Mater. Interfaces*, 2014, 6, 11851-11858.
20 A. S. Subbiah, A. Halder, S. Ghosh, N. Mahuli, G. Hodes and S. K. Sarkar, *J. Phys. Chem. Lett*. 2014, 5, 1748-1753.
21 Z. Wu, S. Bai, J. Xiang, Z. Yuan, Y. Yang, W. Cui, X. Gao, Z. Liu, Y. Jin and B. Sun, *Nanoscale*, 2014, 6, 10505-10510.
22 L. Hu, J. Peng, W. Wang, Z. Xia, J. Yuan, J. Lu, X. Huang, W. Ma, H. Song, W. Chen, Y.-B. Cheng and J. Tang, *ACS Photonics*, 2014, 1, 547-553.
23 Z. Zhu, Y. Bai, T. Zhang, Z. Liu, X. Long, Z. Wei, Z. Wang, L. Zhang, J. Wang, F. Yan and S. Yang, *Angew. Chem. Int. Ed.*, 2014, 53, 12571-12575.
24 J. Seo, S. Park, Y. C. Kim, N. J. Jeon, J. H. Noh, S. C. Yoon and S. I. Seok, *Energy Environ. Sci.*, 2014, 7, 2642-2646.
25 Q. Wang, Y. Shao, Q. Dong, Z. Xiao, Y. Yuan and J. Huang, *Energy Environ. Sci.*, 2014, 7, 2359-2365.
26 H.-B. Kim, H. Choi, J. Jeong, S. Kim, B. Walker, S. Song and J. Y. Kim, *Nanoscale*, 2014, 6, 6670-6683.
27 C. Zuo and L. Ding, *Nanoscale*, 2014, 6, 9935-9938.
28 C.-W. Chen, H.-W. Kang, S.-Y. Hsiao, P.-F. Yang, K.-M. Chiang and H.-W. Lin, *Adv. Mater.*, 2014, 26, 6647-6652.
29 O. Malinkiewicz, C. Roldan-Carmona, A. Soriano, E. Bandiello, L. Camacho, M. K. Nazeeruddin and H. J. Bolink, *Adv. Energy Mater.*, 2014, 4, 1400345.
30 O. Malinkiewicz, A. Yella, Y. H. Lee, G. M. Espallargas, M. Gräztel, M. K. Nazeeruddin and H. J. Bolink, *Nat. Photonics*, 2014, 8, 128-132.
31 Q. Lin, A. Armin, R. C. R. Nagiri, P. L. Burn and P. Meredith, *Nat. Photonics*, 2015, 9, 106-112..
32 J. Burschka, N. Pellet, S.-J. Moon, R. Humphry-Baker, P. Gao,

M. K. Nazeeruddin and M. Gräztel, *Natute*, 2013, 499, 316-319.

33 M. Liu, M. B. Johnston and H. J. Snaith, Nature, 2013, 501, 395-398.

34 P.-W. Liang, C.-Y. Liao, C.-C. Chueh, F. Zuo, S. T. Williams, X.-K. Xin, J. Lin and A. K.-Y. Jen, *Adv. Mater.*, 2014, 26, 3748-3754.

35 B. Conings, L. Baeten, D. D. Dobbelaere, J. D'Haen, J. Manca and H.-G. Boyen, *Adv. Mater.*, 2014, 26, 2041-2046.

36 Y. Wu, A. Aslam, X. Yang, C. Qin, J. Liu, K. Zhang, W. Peng and L. Han, *Energy Environ. Sci.*, 2014, 7, 2934-2938.

37 L. Dou, J. You, Z. Hong, Z. Xu, G. Li, R. A. Street and Y. Yang, *Adv. Mater.*, 2013, 25, 6642-6671.

38 N. R. Armstrong, W. Wang, D. M. Alloway, D. Placencia, E. Ratcliff and M. Brumbach, *Macromol. Rapid Commun*, 2009, 30, 717-731.

39 A. L. Ayzner, C. J. Tassone, S. H. Tolbert and B. J. Schwartz, *J. Phys. Chem. C*, 2009, 113, 20050-20060

40 D. Bi, A. M. El-Zohry, A. Hagfeldt and G. Boschloo, *ACS Appl. Mater. Interfaces.*, 2014, 6, 18751-18757.

41 J.-H. Im, I,-H. Jang, N. Pellet, M. Gräztel and N. G. Park, *Nat. Nanotech.*, 2014, 9, 927-932.

42 L. M. Frass, *J. Appl. Phys.*, 1978, 49, 871-875.

43 D. Liu and T. L. Kelly, *Nat. Photonics*, 2014, 8, 133-138.

44 L. Zheng, Y. Ma, S. Chu, S. Wang, B. Qu, L. Xiao, Z. Chen, Q. Gong, Z. Wu and X. Hou, *Nanoscale*, 2014, 6, 8171-8176.

45 T. Baikie, Y. Fang, J. M. Kadro, M. Schreyer, F. Wei, S. G. Mhaisalkar, M. Graetzel and T. J. White, *J. Mater. Chem. A*, 2013, 1, 5628–5641.